ADVANCED ENERGY MATERIALS
www.advenergymat.de

Harnessing Solar Energy for Ammonia Synthesis from Nitrogen and Seawater Using Oxynitride Semiconductors

Yiyang Li, Mengqi Duan, Simson Wu, Robert A. Taylor, and Shik Chi Edman Tsang**

Green ammonia evolution by photocatalytic means has gained significant attention over recent decades, however, the energy conversion efficiency remains unsatisfactory, and deep mechanistic insights are absent. Here in this work, this challenge is addressed by developing a photothermal system that synthesizes ammonia from nitrogen and natural seawater under simulated solar irradiation, employing ruthenium-doped barium tantalum oxynitride semiconductors. This method significantly enhances solar-to-ammonia conversion efficiency, providing a viable alternative to the energy-intensive Haber–Bosch process. Optimized at 240 °C, the system achieves an ammonia evolution rate of 5869 μmol g^{-1} h^{-1} in natural seawater. Moreover, detailed characterizations have shown that the use of seawater not only leverages an abundant natural resource but also improves the reaction kinetics and overall system stability. The catalysts maintain their activity and structural integrity over multiple cycles, demonstrating both the feasibility and the durability of this innovative system. Achieving a solar-to-ammonia efficiency of 13% and an overall energy conversion efficiency of 6.3%, this breakthrough highlights the potential to decentralize ammonia production, enhancing accessibility and sustainability. This approach combines the benefits of thermal and photocatalytic processes, marking a significant advancement in ammonia synthesis technology.

1. Introduction

Ammonia (NH_3) production through the Haber–Bosch process has significantly contributed to the global population explosion since the early 20th century.[1,2] Recognised for its high volumetric energy density – 2.8 times greater than that of compressed H_2 at 700 bar – NH_3 is also emerging as a promising alternative energy carrier, especially important as the world seeks sustainable energy solutions.[3,4] The conventional production of NH_3 is not only energy-intensive, consuming 1–2% of global fossil fuel reserves, but it also emits ≈300 million tons of CO_2 annually, exacerbating global warming.[5] Therefore, there is a pressing need for a novel NH_3 production process that utilizes renewable energy sources and operates under milder conditions compared to conventional methods. Among different green NH_3 evolution routes, solar-driven photocatalytic N_2 fixation offers a promising strategy. This process utilizes solar energy to drive the reduction of N_2 by H_2O into NH_3 and O_2, a reaction that results in significant free energy gain (Equation 1; Note S1, Supporting Information).

$$0.5\ N_2\ (g) + 1.5\ H_2O\ (l) = NH_3\ (aq) + 0.75\ O_2\ (g) \quad (1)$$

Since the pioneering work in 1977, in which the potential of a TiO_2 photocatalyst for N_2 fixation with water was demonstrated,[6] various semiconductors have been studied for the photocatalytic NH_3 production, such as ZnO, BiOCl, CdS, etc.[7–9] Despite extensive efforts in recent decades, the photocatalytic NH_3 evolution systems often suffer from unsatisfactory solar-to-ammonia conversion efficiency (η_{STA}) and poor stability, primarily due to narrow absorption of solar spectrum, rapid charge carrier recombination, and slow surface reaction kinetics.[10–12]

To address these challenges, researchers have commonly employed strategies including defect engineering and co-catalyst loading. One of the challenging steps for such systems is the chemical adsorption and activation of N_2. For this reason, noble metals such as Ru are frequently used to enhance N_2 activation due to their favorable adsorption energies with N_2.[13–15] Moreover, it has been noted that anion vacancies (e.g., N and

Y. Li, M. Duan, S. C. E. Tsang
Wolfson Catalysis Centre
Department of Chemistry
University of Oxford
Oxford OX1 3QR, UK
E-mail: yiyang.li@chem.ox.ac.uk; edman.tsang@chem.ox.ac.uk
S. Wu
Oxford Green Innotech Limited
Oxford Business Park
Oxford OX4 2HN, UK
R. A. Taylor
Clarendon Laboratory
Department of Physics
University of Oxford
Oxford OX1 3PU, UK

The ORCID identification number(s) for the author(s) of this article can be found under https://doi.org/10.1002/aenm.202406160

DOI: 10.1002/aenm.202406160

O vacancies) alongside adjacent metal ions behave as the N_2 reduction sites, facilitating the N≡N bond stretching and enhancing photocatalytic performance.[16,17] Additionally, the oxygen evolution reaction (OER), which stems from water oxidation in the valence band, is inherently sluggish and thermodynamically unfavorable.[18,19] Our recent work has shown that elevated temperatures can enhance OER by promoting oxygen vacancy generation and increasing lattice oxygen mobility, shifting the OER mechanism to a more efficient lattice oxygen-mediated process.[20–22] Furthermore, in any photocatalytic system, the charge carrier dynamics play a crucial role. The rapid recombination of the photogenerated charge carriers for conventional materials often leads to low η_{STA}. It has been widely accepted that shallow defects can facilitate the separation of the photogenerated charge carriers by inducing mid-gap states, prolonging the charge carrier lifetime.[23,24] These mid-gap states will also contribute to broader visible light absorption.

In light of the findings regarding material design, our study focuses on perovskite oxynitride materials, given by the chemical formula $AB(O,N)_3$, which have been regarded as promising photocatalysts due to their tuneable composition and physicochemical properties.[25] Specifically, $BaTaO_2N$ has exhibited a favorable absorption edge of ≈680 nm.[25,26] The versatility of these materials allows for further enhancement of their electronic properties by substituting different cations, which improves electronic coupling through oxygen atoms.[27] The utilization of seawater instead of pure water in photocatalytic and electrocatalytic applications is gaining attention, given that over 95% of Earth's water resources are saline.[28,29] Although the direct electrolysis of seawater has made great progress in recent years, there are major challenges that are yet to be overcome.[30–32] For instance, for every 1 MW of electrolyzer capacity, at least 2–3 MW of renewable nameplate capacity is needed to accommodate the low capacity factors for the renewables.[33] In sharp contrast, by using one-pot synthesis solely driven by sunlight, such challenges could be overcome. However, the role of ionic species in seawater in photocatalytic systems remains poorly understood and is often debated, necessitating further investigation.

Herein, we present an efficient and robust photothermal NH_3 evolution system employing a Ru-supported perovskite oxynitride catalyst, operated under simulated solar irradiation at elevated temperatures. In this innovative system, both NH_3 and O_2 evolution are boosted simultaneously and are generated stoichiometrically from the abundant N_2 and natural seawater. It is demonstrated that the competing H_2 evolution reaction can be suppressed by tuning the reaction temperature. The system achieves an exceptional NH_3 evolution rate of 5869 μmol g^{-1} h^{-1}, demonstrating robust stability and high durability over multiple cycles. Detailed investigations indicate that the electrolyte species in seawater greatly prolong the charge carrier lifetime and suppress their recombination, due to enhanced local polarisation at elevated temperatures. Additionally, the presence of Cl^- ions has been shown to kinetically facilitate the OER. Elevated temperatures also promote the formation of anion defects, which further improve the catalytic performance. Remarkably, this photothermal system efficiently converts N_2 to NH_3 using natural seawater without requiring any sacrificial agents. A high quantum efficiency (QE) is achieved up to 650 nm and a promising overall energy conversion efficiency of ≈6.3% is demonstrated at 240 °C – the highest reported efficiency among comparable systems.[9–11,34] This approach not only marks a significant advancement in NH_3 synthesis technology by leveraging advanced materials and renewable energy but also holds great potential for decentralizing NH_3 production, thereby enhancing accessibility and environmental sustainability.

2. Results and Discussion

2.1. Material Preparation and Characterizations

We synthesized a series of $MTaO_2N$ (M=Ba, Sr, and Ca) oxynitride perovskite materials using a flux-assisted method adopted from literature,[35–37] denoted as BTON, STON, and CTON, respectively. As shown in **Figure 1a**, the precursors were thoroughly mixed and ground before being placed in a tube furnace. The mixture was then treated with an NH_3 flow at 1000 °C for 8 h to synthesize the oxynitride. Metal nanoparticles were then deposited onto the oxynitride materials using a wet impregnation method, followed by a reduction in an H_2/N_2 flow. Further details on the catalyst preparation are available in the Supporting Information. All materials confirmed a perovskite structure via X-ray diffraction (XRD) patterns. We observed a systematic shift in diffraction peaks toward lower 2θ values from CTON to BTON (Figure 1a), indicative of lattice expansion correlating with the increasing size of A-site cations.[38] Elemental analysis using inductively coupled plasma mass spectrometry (ICP-MS) has verified the composition of the materials (Table S1, Supporting Information). Synchrotron XRD was engaged to gain further structural insights (Figure 1b). Rietveld refinements further confirmed the perovskite structure and stoichiometry of BTON (Table S2, Supporting Information). Transmission electron microscopy (TEM) was then used to investigate these perovskite materials. For example, it shows that BTON consists of agglomerated particles with a mean size of 47±4 nm (Figure 1c,d). UV–vis diffuse reflectance spectroscopy (UV–vis DRS) illustrated a broad light absorption spectrum for BTON, extending up to ≈670 nm, whereas STON and CTON absorbed only up to 590 and 550 nm, respectively (Figure 1e). The corresponding Tauc plots were subsequently derived from the UV–vis DRS spectra to evaluate the bandgap energy, as shown in Figure S1 (Supporting Information). This Tauc plot analysis demonstrates that the bandgap energy of BTON is 1.84 eV, which is consistent with literature values.[36] Further details on Tauc plot analysis can be found in Methods.

X-ray photoelectron spectroscopy (XPS) explored the chemical environment within the perovskites, revealing distinct Ta species and evidencing the integration of nitrogen into the lattice (Figure 1f–h). All materials exhibited a peak at 396.7 eV for N 1s, attributable to lattice N^{3-} (Figure 1f). Two types of Ta species were observed, with the Ta $4f_{7/2}$ binding energy (BE) of 25.6 and 24.5 eV, respectively (Figure 1g). The species with a higher BE can be attributed to Ta^{5+}, while the lower BE agrees well with that of Ta^{4+},[39] originating from the partial reduction of Ta^{5+} during the high-temperature NH_3 treatment. Accordingly, partial reduction of Ta^{5+} will inevitably lead to the formation of oxygen vacancies (O_Vs), leaving five-coordinated Ta sites (denoted as Ta_{5c}). O 1s spectra showed peaks corresponding to various oxygen types at 533.1, 531.5, and 529.6 eV (Figure 1h), which can be assigned to surface hydroxyl groups (O—H), oxygens connected

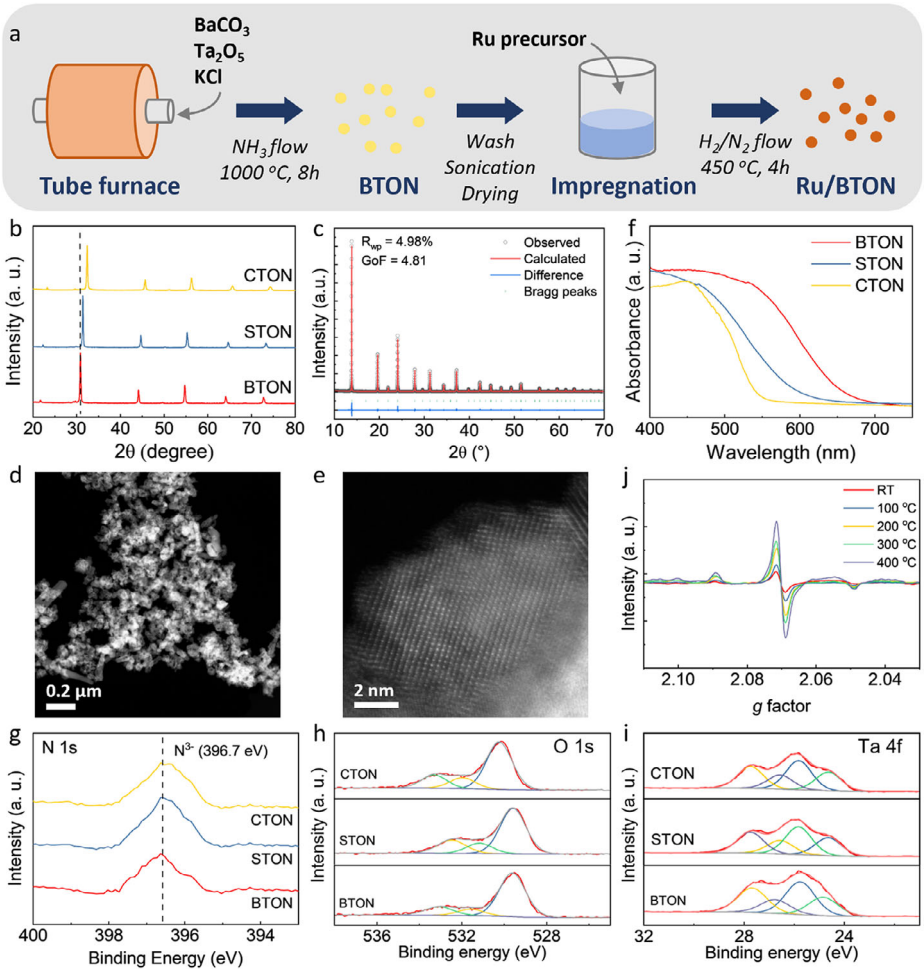

Figure 1. Preparation and characterizations of $MTaO_2N$ (M=Ba, Sr, and Ca) oxynitride perovskite materials. a) Schematic illustration of the Ru/BTON catalyst preparation procedure. b) XRD patterns of CTON, STON, and BTON. XRD patterns indicate that all materials show a similar perovskite phase. c) SXRD spectrum and fitting of BTON. d,e) low-magnification and high-magnification TEM images of BTON. f) UV–vis spectra of CTON, STON, and BTON. g–i) N 1s, O 1s, and Ta 4f XPS spectra of CTON, STON, and BTON. All XPS spectra were calibrated with respect to the C 1s peak (binding energy = 284.8 eV). j) EPR spectra of BTON obtained at different temperatures. EPR spectra suggest the presence of surface oxygen vacancies.

to Ta_{5c} (i.e., O-Ta_{5c}) and lattice oxygens ($O_{lattice}$), respectively.[40] It is also observed that these properties do not show much dependence on the A-site cation. In addition, electron paramagnetic resonance (EPR) spectroscopy further evidences the presence of surface defects in BTON (Figure 1i). The signal at $g \approx 2.07$ is attributed to the O_2^- resulted from O_2 sitting at surface anion vacancy sites.[41,42] Surface anion vacancies, such as O and N vacancies, are considered the active sites for the OER and N_2 adsorption and activation.[16,43–45] Moreover, the concentration of these surface defects shows a strong positive dependence on temperature. This facilitated generation of surface anion vacancies at elevated temperatures will then promote the OER and N_2 activation significantly, hence giving enhanced activity.

2.2. Photothermal NH_3 Evolution at Elevated Temperatures

We first studied the relationship between Gibbs free energy changes and temperature for the NH_3 evolution reaction and water splitting reaction (**Figure 2a**). While both reactions are thermodynamically unfavorable, increasing temperatures reduce the Gibbs free energy changes. It should be noted that water splitting is thermodynamically more favorable than the NH_3 evolution reaction (Figure 2a). Subsequently, the effect of temperature on photothermal NH_3 evolution was studied over a temperature range of 150 to 300 °C, as shown in Figure 2b. The reaction was carried out in a batch reactor in the presence of pure nitrogen and pure water. Our control experiments confirmed that this reaction cannot take place at room temperature or without light irradiation (Table S3, Supporting Information). It is also shown that the activity greatly relies on the mass of the catalyst used and the light irradiance (Figure S2, Supporting Information), and thus the experimental conditions are optimized. We have also employed gas chromatography and UV–vis spectroscopy to identify other potential N_2 oxidation or reduction products. These analyses have confirmed that NH_3 is the only N-containing product in this system. Further details on the product analysis are provided in the Methods section. It should be emphasized that during the prepa-

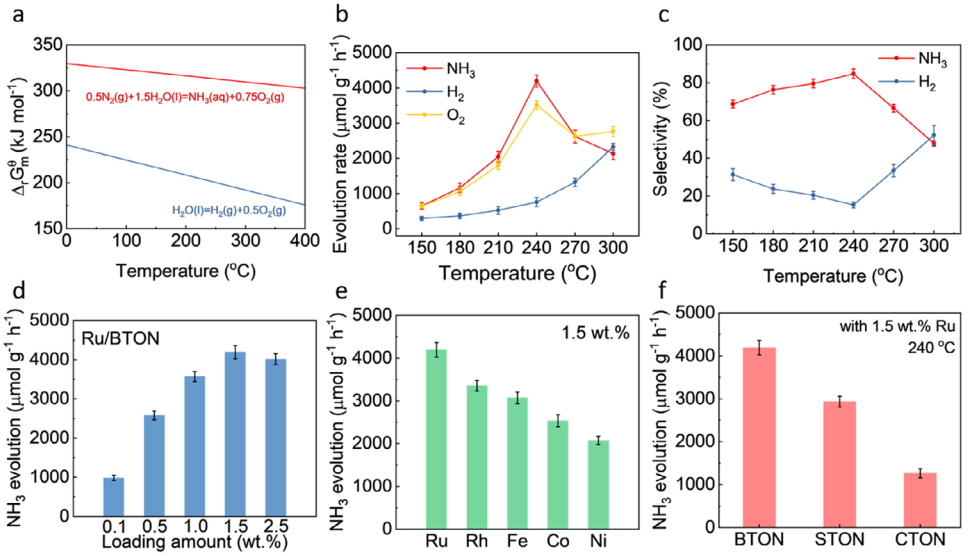

Figure 2. Evaluation of the photothermal NH3 evolution performance over oxynitride perovskite catalysts. a) Temperature dependences of the changes in the Gibbs free energy of NH_3 evolution and water splitting. b) Evolution rates of NH_3, H_2, and O_2 as a function of temperature over Ru/BTON. c) Product selectivity of NH_3, H_2, and O_2 as a function of temperature over Ru/BTON. d) Optimisation of Ru loading amount. e) Optimisation of metal co-catalyst. f) the NH_3 evolution performance of different Ru-supported oxynitride perovskite catalysts.

ration of materials, we made deliberate efforts to avoid using N-containing precursors, and all catalysts were thoroughly washed with deionized water prior to use.[46]

Figure 2b illustrates that the activity of the oxynitride perovskite materials is highly dependent on the reaction temperature. As shown before, elevated temperatures notably facilitate the generation of surface anion defects, which is beneficial for OER and N_2 adsorption and activation. The evolution of H_2 from water splitting positively correlates with increasing temperature and is barely detectable at temperatures below 150 °C. In contrast, NH_3 evolution activity is substantially enhanced at elevated temperatures and peaks at ≈240 °C under simulated solar irradiation, achieving a high NH_3 evolution rate of 4194 μmol g^{-1} h^{-1}, and then declines sharply with further temperature increases for the Ru-supported BTON (denoted as Ru/BTON). Throughout all catalytic tests in this work, the reaction stoichiometry has been analyzed meticulously. The molar amounts of the produced NH_3, H_2, and O_2 adhere to the relationship demonstrated in Equation 2

$$3 \times n\left(NH_3\right) + 2 \times n\left(H_2\right) = 4 \times n\left(O_2\right) \quad (2)$$

Our previous work established that the photocatalytic overall water splitting (POWS) reaction also occurs under these experimental conditions,[20–22] competing with the N_2 reduction reaction. H_2 evolution is a relatively facile process, while oxygen evolution is kinetically challenging, being a four-electron process that requires a high overpotential.[47] Therefore, the competition between the POWS reaction and photothermal NH_3 evolution is central to understanding the trends observed in Figure 2b. Protons and N_2 molecules compete for the photogenerated electrons in the conduction band, while H_2O/OH^- consumes the photogenerated holes in the valence band. At temperatures below 150 °C, H_2 evolution from water splitting is minimal. As temperature increases, both reactions are thermodynamically facilitated (Figure 2a), and the ionic dissociation of water enhances, notably peaking between 260–270 °C before sharply declining at higher temperatures.[48] This results in a higher proton concentration, thus improving the kinetics for H_2 evolution. Conversely, higher temperatures reduce the adsorption of N_2 on the catalyst surface, adversely affecting photothermal NH_3 evolution. The selectivity for NH_3 and H_2, as shown in Figure 2c, indicates that the two reactions can be kinetically tuned by adjusting the reaction temperature. NH_3 evolution is significantly enhanced at elevated temperatures, peaking at ≈240 °C under simulated solar irradiation, then sharply declining as temperature increases further with the Ru/BTON catalyst. At 240 °C, NH_3 evolution is optimized, while H_2 evolution remains suppressed. However, at higher temperatures (i.e., 240–270 °C), the increased concentration of protons facilitates H_2 evolution, preferentially consuming the photogenerated electrons in the valence band, which substantially competes with NH_3 formation due to unfavorable N_2 adsorption on the catalyst surface (i.e., Ru sites). In the meantime, the OER is also facilitated kinetically by an increased number of O_Vs, as evidenced by EPR results (Figure 1j), while NH_3 evolution becomes negligible. Similar volcanic trends have also been observed in prior work.[15] In addition, it is also possible that the NH_3 oxidation and decomposition become more facile at higher temperatures above 270 °C.

The deposition of metal co-catalysts was also investigated, including Ru, Rh, Fe, Co, and Ni, all of which are traditionally considered as good cocatalysts for N_2 activation (Figure 2d,e). Each metal demonstrated enhanced activity to varying extents, with Ru exhibiting the highest NH_3 evolution rate of 4194 μmol g^{-1} h^{-1} at 240 °C, presumably due to its favorable adsorption energy with N_2. Notably, non-noble metal co-catalysts also showed promise, with Fe/BTON achieving an activity of 3071 μmol g^{-1} h^{-1}. The loading percentage of Ru on BTON was then

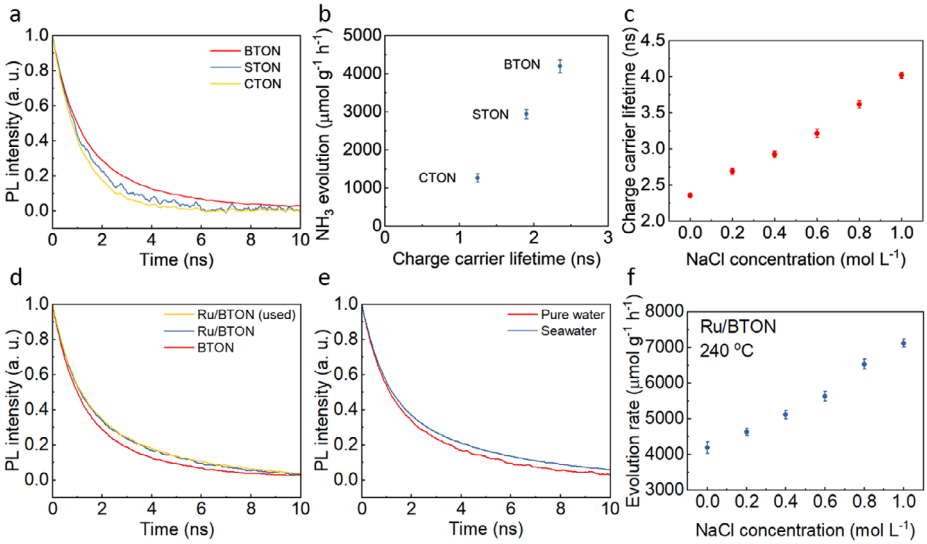

Figure 3. Investigation of photogenerated charge carrier dynamics. a) TRPL spectra of BTON, STON, and CTON with an excitation wavelength of 266 nm. b) Correlation between NH_3 evolution activity and charge carrier lifetime for BTON, STON, and CTON. c) Relationship between the charge carrier lifetime of BTON and the concentration of NaCl in aqueous solutions. d) TRPL spectra comparison of BTON, fresh Ru/BTON, and used Ru/BTON. Used Ru/BTON refers to the catalyst after undergoing the long-term stability test. e) TRPL spectra of Ru/BTON in pure water versus natural seawater. f) Correlation between photothermal activity and NaCl concentration in aqueous solutions. Error bars represent standard deviations.

optimized (Figure 2e). Figure 2f indicates that BTON outperforms other materials in the prepared oxynitride series, primarily due to its broad absorption range and facilitated generation of surface anion vacancies.

The Ru/BTON catalyst has been comprehensively characterized to confirm the successful loading of metal nanoparticles. ICP-MS analysis confirmed the Ru concentration at ≈1.5 wt.%, aligning with the intended loading concentration (Table S1b, Supporting Information). XRD confirmed that Ru loading did not induce significant structural changes, preserving the perovskite lattice structure. Additionally, the XRD patterns showed no additional peaks for Ru nanoparticles, suggesting their small size (Figure S3a, Supporting Information). TEM revealed homogeneously dispersed Ru nanoparticles on the BTON surface, with an average particle size of 2.4±0.3 nm (Figure S4, Supporting Information). UV–vis DRS demonstrated no additional absorption features after Ru loading, and the bandgap energy remained unchanged, as evidenced by the Tauc plot analysis (Figure S1, Supporting Information). Moreover, XPS also confirmed the successful loading of Ru nanoparticles. The XPS spectra have been carefully deconvoluted to assess the chemical environment of Ru, revealing that most Ru is in the oxidation state of zero, with other species possibly in the Ru(II) state due to surface oxidation (Figure S3, Supporting Information).[13,14] Additionally, valence band XPS spectra have shown that the Ru loading does not influence the position of the valence band. Post-reaction characterizations were also meticulously performed using XRD, XPS, UV–vis DRS, ICP-MS, and TEM, showing no significant changes compared to the fresh Ru/BTON catalyst (Figures S1 and S3, and S4, Supporting Information).

Time-resolved photoluminescence (TRPL) spectroscopy was subsequently used to investigate the dynamics of the photoexcited charge carriers. As shown in **Figure 3a**, the charge carrier lifetime follows the trend: BTON>STON>CTON, which aligns well with the NH_3 evolution rate. It is widely recognized that the separation of photoexcited charge carriers plays an important role in photocatalysis. The NH_3 evolution rate is thus plotted against the charge carrier lifetime, showing a clear linear correlation (Figure 3b). Clearly, the prolonged charge carrier lifetime allows for the surface chemical reactions to take place. Subsequently, we also attempted to explore the effect of reaction temperature on photothermal activity using TRPL. While the charge carrier lifetime shows no significant change across the temperature range studied, it is notably influenced by varying the concentration of ionic species in the water. NaCl was used as an example, which indicated that the increased NaCl concentrations could substantially prolong the charge carrier lifetime of BTON, presumably due to the electrolyte-assisted polarisation effect.[20,22] A linear correlation can be observed between the charge carrier lifetime and NaCl concentration, as shown in Figure 3c. As a result, the lifetime of 2.35 ns in pure water is prolonged to 4.13 ns in a 1.0-mol L^{-1} NaCl aqueous solution. As discussed before, the ionic dissociation of water is facilitated at elevated temperatures, which means the concentration of ionic species in water (i.e., H^+ and OH^-) is increased substantially. Therefore, we can expect a greatly prolonged charge carrier lifetime at elevated temperatures even without any additional electrolytes. This suggests that a strong polarisation is induced near the catalyst surface by higher concentrations of H^+ and OH^- ions, interacting with charge carriers of the counter charge within the catalyst particles. This interaction then suppresses the recombination and enhances photocatalytic performance.

2.3. Photothermal NH_3 Evolution Using Seawater

Building on the findings of prolonged charge carrier lifetime in NaCl solution (Figure 3b), we subsequently explored the pho-

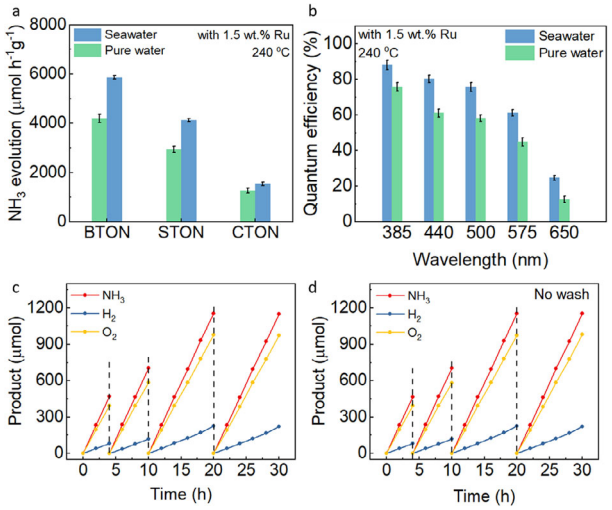

Figure 4. Evaluation of NH_3 evolution performance in natural seawater. a) NH_3 evolution rate comparison of 1.5 wt.% Ru-supported oxynitride perovskite catalysts in pure water and natural seawater at 240 °C under AM 1.5G simulated solar irradiation. b) QE evaluations of the 1.5 wt.% Ru/BTON catalyst in pure water and natural water at different wavelengths at 240 °C. Error bars represent standard deviations. c) Four-cycle stability test of 1.5 wt.% Ru/BTON in natural seawater at 240 °C, totaling 30 h of reaction time. The photocatalyst was recycled by centrifugation, washed with Milli-Q water, and dried at 60 °C under vacuum for 10 h before reuse. d) Stability test of 1.5 wt.% Ru/BTON in natural seawater at 240 °C without washing between cycles to assess the impact of residual sea salt.

tothermal NH_3 evolution using natural seawater as a substitute for pure water. Remarkably, the oxynitride perovskite catalysts demonstrated more efficient NH_3 evolution in natural seawater (**Figure** 4a) due to the electrolyte-assisted polarisation effect induced by the ionic species in seawater.[20] We have also previously demonstrated that such an electrolyte-assisted effect becomes more significant at elevated temperatures. Consequently, the NH_3 evolution rate is improved to 5869 μmol g^{-1} h^{-1}, marking a notable enhancement of ≈40% compared to that in pure water. The TRPL results clearly demonstrated that the charge carrier lifetime is significantly extended upon Ru loading, which is likely due to electron trapping within Ru nanoparticles, resulting in a polarisation of charges (Figure 3d). Moreover, the charge carrier lifetime of BTON in natural seawater was notably increased to 3.26 ns, closely matching that observed in a 0.6 mol L^{-1} NaCl solution (Figure 3c,e). In addition, the photothermal activity was assessed in NaCl aqueous solutions of various concentrations. As illustrated in Figure 3f, a clear linear correlation with NaCl concentration was established, further substantiating the electrolyte-assisted polarisation effect. Electrochemical impedance spectroscopy was also employed to evaluate the charge transfer resistance, revealing a substantial reduction in resistance in natural seawater compared to pure water (Figure S5, Supporting Information).

A significant concern with using natural seawater in photocatalytic systems is the potential reduction of chloride ions to toxic Cl-containing chemicals. In this system, the presence of oxidative Cl-containing species may also oxidize the produced NH_3, lowering the overall photothermal activity. It should be mentioned that the photocatalytic oxidation of Cl^- in seawater has not been understood well.[49] It is believed that Cl^- ions react with the photogenerated holes to produce Cl_2 or HClO. In addition, it is kinetically easier for the oxidation of Cl^- to produce Cl_2 than H_2O oxidation to O_2 (Equation 3).[50] Therefore, extensive efforts have been made for the quantification of chlorine. Gas chromatography confirmed no gaseous Cl_2 formation post-reaction. We also carefully analyzed the chlorine balance before and after the reaction using titration. We meticulously analyzed the chlorine balance using titration, confirming that the concentrations of Cl^- remained consistent before and after the reaction, within experimental uncertainty. To assess the presence of any dissolved Cl_2 or HClO, we scrutinized the post-reaction solution by adding a potassium iodide solution and starch as an indicator, with no detectable color change observed, suggesting the absence of oxidative Cl_2 or HClO species in the solution. Actually, if Cl_2 is generated during the reaction, it would easily dissolve in and react with water to form HClO (Equation 4). HClO will then readily decompose into Cl^- under irradiation (Equation 5),[51] especially at elevated temperatures. Therefore, it is difficult to detect the presence of Cl_2 gas under our photothermal condition. Actually, if the reaction proceeds via Equations (3)–(5), the net effect is that Cl^- is not consumed but acts as a catalyst to facilitate the OER, given that the photocatalytic oxidation of Cl^- is kinetically favorable.

$$2Cl^- + 2h^+ = Cl_2 \quad (3)$$

$$Cl_2 + H_2O = HCl + HClO \quad (4)$$

$$2HClO = 2HCl + O_2 \quad (5)$$

Quantum efficiency (QE) is a critical parameter for evaluating photon-to-chemical conversion in renewable solar conversion systems. Almost all the reported photocatalytic NH_3 evolution systems suffer from an extremely low QE, especially in the visible-light regime, which largely hinders further practical applications.[10,11,34] In our system, the QE was evaluated at 240 °C at different wavelengths by using band-pass filters. Remarkably, a high average QE over the whole visible regime was achieved in natural seawater for all Ru-supported oxynitride perovskite catalysts. Specifically, the Ru/BTON catalyst exhibited an exceptional QE of 88.1% at 385 nm in natural seawater, with a noteworthy QE of 24.8% at 650 nm (i.e., close to the absorption edge of BTON). It is shown that the QE decreases at longer wavelengths, which can presumably be attributed to the wavelength-dependent electron–hole pair generation: the absorbed photons at a longer wavelength may not generate excited electron-hole pairs, but excite local transitions instead.[52] Additionally, high-energy photons may promote charge separation and enhance electron-phonon coupling,[53] whereas long-wavelength excitation tends to lead to increased local polaron formation, reducing the mobility of the charge carriers and consequently decreasing the number of carriers reaching the catalyst surface.[54]

The stability of the Ru/BTON catalyst was further investigated by recycling it four times over a total reaction time of 30 h (Figure 4c). The results have demonstrated a continuous and stoichiometric evolution of NH_3, O_2, and H_2, with no notable drop of activity, indicating the catalyst's robust stability. Additionally, we explored the potential impact of residual sea salt on the photocatalyst's performance. In a similar stability test where the pho-

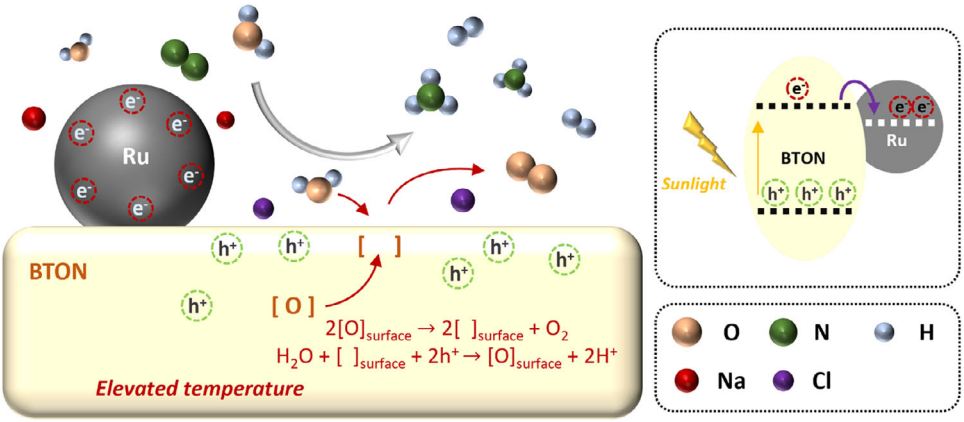

Figure 5. Schematic illustration of the photothermal NH_3 evolution mechanism in seawater using the Ru/BTON catalyst.

tocatalyst was not washed between cycles, no noticeable change in reaction performance was observed, as depicted in Figure 4d. This indicates that the residual sea salt has a negligible influence on the catalytic activity. Subsequently, we evaluated the energy conversion of solar energy into chemical energy. While the conventional η_{STA} is typically measured at room temperature and ambient pressure, our experiments were conducted at elevated temperatures and pressures. As a result, we defined a photon-to-ammonia energy conversion efficiency at the specific evaluation temperature of 240 °C, denoted as $\eta_{PTA}(240°C)$. This measure is particularly useful as it highlights the catalyst's capacity to convert photon energy directly into chemical energy under specified conditions, excluding other technical factors like heat loss. The energy required to reach and maintain this temperature can be supplied by various means, including electrical or microwave heating. In this context, our system achieved a notable $\eta_{PTA}(240°C)$ of $13.03 \pm 0.42\%$ in natural seawater at 240 °C (Note S1, Supporting Information). Furthermore, we evaluated the overall energy conversion efficiency (η_{OEC}) by accounting for the energy necessary to heat and maintain the reaction system at the required temperature. A very promising η_{OEC} of $6.3 \pm 0.3\%$ was demonstrated. In an ideal future design, we anticipate that the energy for heating could be provided by concentrated solar light so that the energy consumption for heating may be minimized or even excluded in that scenario, thus a higher η_{OEC} could be expected.

Figure 5 illustrates the proposed mechanism for the photothermal NH_3 evolution reaction investigated in this study. Upon irradiation with simulated solar light, excitation results in the generation of electrons and holes. These charge carriers then migrate to different surface sites, with electrons favorably localized on the Ru nanoparticles and holes on the BTON surface, thereby establishing charge polarization. As demonstrated in our previous work,[20] ionic species in seawater, such as Na^+ and Cl^-, are likely to adsorb onto different regions of the photocatalyst via electrostatic attractions, enhancing the separation of the photogenerated charge carriers. This interaction between the ions and charge carriers stabilizes the charge carrier dynamics, leading to an extended lifetime of the charge carriers, as evidenced by the TRPL results (Figure 3). Consequently, N_2 molecules interact with the trapped photogenerated electrons on the Ru nanoparticles, facilitating NH_3 evolution. It can be further deduced that these trapped electrons are able to weaken the N≡N triple bond, making nitrogen more prone to protonation. On the other hand, the OER takes place on the BTON surface, where surface oxygen reacts with the photogenerated holes to form O_2 molecules, leaving O_Vs on the surface. These surface O_Vs can be replenished either by the surrounding water molecules or the oxygen migrated from the sub-surface layers, as illustrated in Figure 5. Although the generation of surface O_Vs and intra-lattice oxygen migration are typically challenging under ambient conditions, these processes are considerably enhanced at elevated temperatures, thereby boosting OER activity. Furthermore, the facilitated charge polarisation may also help to stabilize the protonated intermediates such as Ru–N–N–H species. Additionally, protons may also capture electrons from the Ru nanoparticles, which competes with NH_3 evolution. This side reaction is boosted when the temperature exceeds 240 °C due to the higher proton concentration and the decreased N_2 adsorption.

3. Conclusion

In conclusion, this work successfully demonstrates the feasibility of a metal-supported perovskite oxynitride catalyst system for efficient photothermal NH_3 evolution from nitrogen and natural seawater. The optimal activity was achieved with a 1.5 wt.% Ru-supported barium tantalum oxynitride catalyst, exhibiting an NH_3 evolution rate of 5869 $\mu mol\, g^{-1}\, h^{-1}$ at 240 °C under simulated solar irradiation, with a notable quantum efficiency of 88.1% at 385 nm and an overall energy conversion efficiency of 6.3%. These results signify not only a substantial improvement over traditional methods but also highlight the system's ability to leverage natural seawater, enhancing both environmental sustainability and process efficiency. Furthermore, the extended charge carrier lifetime at elevated temperatures, coupled with the facilitated oxygen evolution reaction due to the ionic species in seawater. Our findings suggest that this technology could be pivotal in decentralizing NH_3 production and reducing reliance on centralized chemical plants and fossil fuels. The robustness and scalability of this system hold great promise for contributing to a greener and more sustainable future in chemical manufacturing.

Supporting Information

Supporting Information is available from the Wiley Online Library or from the author.

Acknowledgements

The authors acknowledge the support for this project from the EPSRC in the UK (EP/K040375/1).

Conflict of Interest

The authors declare no conflict of interest.

Author Contributions

Y.L. prepared, characterized tested the catalysts performed TRPL experiments, and analyzed the data with the help of RAT, and wrote the paper in discussion with S.W. and other authors. MD performed the Rietveld refinement of SXRD results. S.C.E.T. supervised the overall project.

Data Availability Statement

The data that support the findings of this study are available from the corresponding author upon reasonable request.

Keywords

nitrogen fixation, perovskite oxynitride, photocatalysis, photothermal ammonia evolution

Received: December 30, 2024
Revised: March 7, 2025
Published online: March 17, 2025

[1] J. Liu, M. S. Kelley, W. Wu, A. Banerjee, A. P. Douvalis, J. Wu, Y. Zhang, G. C. Schatz, M. G. Kanatzidis, *Chemistry* **2016**, *113*, 5530.
[2] P. Avenier, M. Taoufik, A. Lesage, X. Solans-Monfort, A. Baudouin, A. De Mallmann, L. Veyre, J. M. Basset, O. Eisenstein, L. Emsley, E. A. Quadrelli, *Science* **2007**, *317*, 1056.
[3] J. G. Chen, R. M. Crooks, L. C. Seefeldt, K. L. Bren, R. M. Bullock, M. Y. Darensbourg, P. L. Holland, B. Hoffman, M. J. Janik, A. K. Jones, M. G. Kanatzidis, P. King, K. M. Lancaster, S. V. Lymar, P. Pfromm, W. F. Schneider, R. R. Schrock, *Science* **2018**, *360*, 873.
[4] B. Lin, L. Heng, B. Fang, H. Yin, J. Ni, X. Wang, J. Lin, L. Jiang, *ACS Catal.* **2019**, *9*, 1635.
[5] S. Licht, B. Cui, B. Wang, F. F. Li, J. Lau, S. Liu, *Science* **2014**, *345*, 637.
[6] G. N. Schrauzer, T. D. Guth, *J. Am. Chem. Soc.* **1977**, *99*, 7189.
[7] M. Cheng, C. Xiao, Y. Xie, *J. Mater. Chem. A* **2019**, *7*, 19616.
[8] D. Yan, H. Li, C. Chen, Y. Zou, S. Wang, *Small Methods* **2019**, *3*, 1800331.
[9] X. Chen, N. Li, Z. Kong, W. J. Ong, X. Zhao, *Mater. Horiz.* **2018**, *5*, 9.
[10] Q. Han, H. Jiao, L. Xiong, J. Tang, *Mater. Adv.* **2021**, *2*, 564.
[11] D. Mateo, A. Sousa, M. Zakharzhevskii, J. Gascon, *Green Chem.* **2023**, *26*, 1041.
[12] H. M. Nguyen, F. Gorky, S. Guthrie, M. L. Carreon, *Catal. Today* **2023**, *418*, 114141.
[13] S. Wu, K. Y. Tseng, R. Kato, T. S. Wu, A. Large, Y. K. Peng, W. Xiang, H. Fang, J. Mo, I. Wilkinson, Y. L. Soo, G. Held, K. Suenaga, T. Li, H. Y. T. Chen, S. C. E. Tsang, *J. Am. Chem. Soc.* **2021**, *143*, 9105.
[14] S. Wu, Y.-K. Peng, A. I. Large, J. Zheng, T. Chen, H. Duan, I. J. McPherson, I. Wilkinson, H.-L. Chou, G. Held, S. C. E. Tsang, *ACS Catal.* **2020**, *10*, 5614.
[15] J. Zheng, L. Lu, K. Lebedev, S. Wu, P. Zhao, I. J. McPherson, T. S. Wu, R. Kato, Y. Li, P. L. Ho, G. Li, L. Bai, J. Sun, D. Prabhakaran, R. A. Taylor, Y. L. Soo, K. Suenaga, S. C. E. Tsang, *Chem Catal.* **2021**, *1*, 162.
[16] B. M. Comer, Y. H. Liu, M. B. Dixit, K. B. Hatzell, Y. Ye, E. J. Crumlin, M. C. Hatzell, A. J. Medford, *J. Am. Chem. Soc.* **2018**, *140*, 15157.
[17] H. Hirakawa, M. Hashimoto, Y. Shiraishi, T. Hirai, *J. Am. Chem. Soc.* **2017**, *139*, 10929.
[18] T. Hisatomi, J. Kubota, K. Domen, *Chem. Soc. Rev.* **2014**, *43*, 7520.
[19] A. Kudo, Y. Miseki, *Chem. Soc. Rev.* **2009**, *38*, 253.
[20] Y. Li, H. Zhou, S. Cai, D. Prabhakaran, W. Niu, A. Large, G. Held, R. A. Taylor, *Nat. Catal.* **2024**, *7*, 77.
[21] C. Foo, Y. Li, K. Lebedev, T. T. Chen, S. Day, C. Tang, S. C. E. Tsang, *Nat. Commun.* **2021**, *12*, 661.
[22] Y. Li, Y.-K. Peng, L. Hu, J. Zheng, D. Prabhakaran, S. Wu, T. J. Puchtler, M. Li, K.-Y. Wong, R. A. Taylor, S. C. E. Tsang, *Nat. Commun.* **2019**, *10*, 4421.
[23] H. Li, J. Shang, Z. Ai, L. Zhang, *J. Am. Chem. Soc.* **2015**, *137*, 6393.
[24] Y. Zhao, Y. Zhao, G. I. N. Waterhouse, L. Zheng, X. Cao, F. Teng, L. Z. Wu, C. H. Tung, D. O'Hare, T. Zhang, *Adv. Mater.* **2017**, *29*, 1703828.
[25] S. Balaz, S. H. Porter, P. M. Woodward, L. J. Brillson, *Chem. Mater.* **2013**, *25*, 3337.
[26] Y. Kim, P. M. Woodward, K. Z. Baba-Kishi, C. W. Tai, *Chem. Mater.* **2004**, *16*, 1267.
[27] B. Zhao, L. Zhang, D. Zhen, S. Yoo, Y. Ding, D. Chen, Y. Chen, Q. Zhang, B. Doyle, X. Xiong, M. Liu, *Nat. Commun.* **2017**, *8*, 14586.
[28] J. Zhang, W. Hu, S. Cao, L. Piao, *Nano Res.* **2020**, *13*, 2313.
[29] A. I. Osman, N. Mehta, A. M. Elgarahy, M. Hefny, A. Al-Hinai, A. H. Al-Muhtaseb, D. W. Rooney, *Environ. Chem. Lett.* **2022**, *20*, 153.
[30] H. Jin, X. Wang, C. Tang, A. Vasileff, L. Li, A. Slattery, S. Z. Qiao, *Adv. Mater.* **2021**, *33*, 2007508.
[31] T. E. Culp, B. Khara, K. P. Brickey, M. Geitner, T. J. Zimudzi, J. D. Wilbur, S. D. Jons, A. Roy, M. Paul, B. Ganapathysubramanian, A. L. Zydney, M. Kumar, E. D. Gomez, *Science* **2021**, *371*, 72.
[32] M. Di Vincenzo, A. Tiraferri, V. E. Musteata, S. Chisca, R. Sougrat, L. B. Huang, S. P. Nunes, M. Barboiu, *Nat. Nanotechnol.* **2021**, *16*, 190.
[33] M. Kibria, M. A. Khan, T. A. Al-Attas, S. Roy, M. M. Rahman, N. Ghaffour, V. Thangadurai, S. Larter, J. Hu, P. Ajayan, *Energy Environ. Sci.* **2021**, *14*, 4831.
[34] L. Wang, M. Xia, H. Wang, K. Huang, C. Qian, C. T. Maravelias, G. A. Ozin, *Joule* **2018**, *2*, 1055.
[35] M. Hojamberdiev, R. Vargas, F. Zhang, K. Teshima, M. Lerch, *Adv. Sci.* **2023**, *10*, 2305179.
[36] Z. Wang, Y. Luo, T. Hisatomi, J. J. M. Vequizo, S. Suzuki, S. Chen, M. Nakabayashi, L. Lin, Z. Pan, N. Kariya, A. Yamakata, N. Shibata, T. Takata, K. Teshima, K. Domen, *Nat. Commun.* **2021**, *12*, 1005.
[37] Y. Luo, S. Suzuki, Z. Wang, K. Yubuta, J. J. M. Vequizo, A. Yamakata, H. Shiiba, T. Hisatomi, K. Domen, K. Teshima, *ACS Appl. Mater. Interfaces* **2019**, *11*, 22264.
[38] D.-Y. Lu, T. Ogata, H. Unuma, X. C. Li, N. N. Li, X. Y. Sun, *Solid State Ionics* **2011**, *201*, 6.
[39] Z. Awaludin, M. Safuan, T. Okajima, T. Ohsaka, *J. Mater. Chem. A* **2015**, *3*, 16791.
[40] X. Liu, J. Mi, L. Shi, H. Liu, J. Liu, Y. Ding, J. Shi, M. He, Z. Wang, S. Xiong, Q. Zhang, Y. Liu, Z. S. Wu, J. Chen, J. Li, *Angew. Chem., Int. Ed.* **2021**, *60*, 26747.
[41] M. Setvín, U. Aschauer, P. Scheiber, Y. F. Li, W. Hou, M. Schmid, A. Selloni, U. Diebold, *Science* **2013**, *341*, 988.
[42] E. Carter, A. F. Carley, D. M. Murphy, *J. Phys. Chem. C* **2007**, *111*, 10630.

[43] A. Kumar, M. Kumar, V. N. Rao, M. V. Shankar, S. Bhattacharya, V. Krishnan, *J. Mater. Chem. A* **2021**, *9*, 17006.
[44] A. Kumar, M. Sharma, S. Sheoran, S. Jaiswal, A. Patra, S. Bhattacharya, V. Krishnan, *Nanoscale* **2023**, *15*, 11667.
[45] M. Sharma, A. Kumar, D. Gill, S. Jaiswal, A. Patra, S. Bhattacharya, V. Krishnan, *ACS Appl. Mater. Interfaces* **2023**, *15*, 55765.
[46] A. Kumar, V. Krishnan, *Adv. Sustainable Syst.* **2024**, *8*, 2400173.
[47] A. Grimaud, O. Diaz-Morales, B. Han, W. T. Hong, Y. L. Lee, L. Giordano, K. A. Stoerzinger, M. T. M. Koper, Y. Shao-Horn, *Nat. Chem.* **2017**, *9*, 457.
[48] A. V. Bandura, S. N. Lvov, *J. Phys. Chem. Ref. Data* **2006**, *35*, 15.
[49] Y. Shiraishi, M. Hashimoto, K. Chishiro, K. Moriyama, S. Tanaka, T. Hirai, *J. Am. Chem. Soc.* **2020**, *142*, 7574.
[50] X. Guan, F. A. Chowdhury, N. Pant, L. Guo, L. Vayssieres, Z. Mi, *J. Phys. Chem. C* **2018**, *122*, 13797.
[51] W. Luo, Z. Yang, Z. Li, J. Zhang, J. Liu, Z. Zhao, Z. Wang, S. Yan, T. Yu, Z. Zou, *Energy Environ. Sci.* **2011**, *4*, 4046.
[52] D. A. Grave, D. S. Ellis, Y. Piekner, M. Kölbach, H. Dotan, A. Kay, P. Schnell, R. van de Krol, F. F. Abdi, D. Friedrich, A. Rothschild, *Nat. Mater.* **2021**, *20*, 833.
[53] Z. Ye, X. Lin, N. Wang, J. Zhou, M. Zhu, H. Qin, X. Peng, *Nat. Commun.* **2021**, *12*, 4283.
[54] L. M. Carneiro, S. K. Cushing, C. Liu, Y. Su, P. Yang, A. P. Alivisatos, S. R. Leone, *Nat. Mater.* **2017**, *16*, 819.